The Calculation of the Vibrational Frequencies of Crystalline Compounds and Its Implementation in the CRYSTAL Code

F. PASCALE,[1] C. M. ZICOVICH-WILSON,[2] F. LÓPEZ GEJO,[3] B. CIVALLERI,[3]
R. ORLANDO,[4] R. DOVESI[3,5]

[1]*Laboratoire de Pétrologie, Modélisation de Matériaux et Processus, Université Pierre et Marie Curie, 4, Place Jussieu, 75232 Paris cedex 05, France*
[2]*Facultad de Ciencias, Universidad Autónoma del Estado de Morelos, Av. Universidad 1001, Col. Chamilpa, 62210 Cuernavaca (Morelos), Mexico*
[3]*Dipartimento di Chimica IFM, Università di Torino, Via P. Giuria 7, 10125 Torino, Italy*
[4]*Dipartimento di Scienze e Tecnologie Avanzate, Università del Piemonte Orientale, C.so Borsalino 54, 15100 Alessandria, Italy*
[5]*Unità INFM di Torino, Sezione F, Via P. Giuria 7, 10125 Torino, Italy*

Received 20 October 2003; Accepted 3 December 2003

Abstract: The problem of numerical accuracy in the calculation of vibrational frequencies of crystalline compounds from the hessian matrix is discussed with reference to α-quartz (SiO_2) as a case study and to the specific implementation in the CRYSTAL code. The Hessian matrix is obtained by numerical differentiation of the analytical gradient of the energy with respect to the atomic positions. The process of calculating vibrational frequencies involves two steps: the determination of the equilibrium geometry, and the calculation of the frequencies themselves. The parameters controlling the truncation of the Coulomb and exchange series in Hartree–Fock, the quality of the grid used for the numerical integration of the Exchange-correlation potential in Density Functional Theory, the SCF convergence criteria, the parameters controlling the convergence of the optimization process as well as those controlling the accuracy of the numerical calculation of the Hessian matrix can influence the obtained vibrational frequencies to some extent. The effect of all these parameters is discussed and documented. It is concluded that with relatively economical computational conditions the uncertainty related to these parameters is smaller than 2–4 cm^{-1}. In the case of the Local Density Approximation scheme, comparison is possible with recent calculations performed with a Density Functional Perturbation Theory method and a plane-wave basis set.

 J Comput Chem 25: 888–897, 2004

Key words: CRYSTAL code; vibrational frequencies; crystalline compounds; a-quartz

Introduction

Vibrational analysis by means of the complementary infrared and Raman spectroscopic techniques is extremely useful for obtaining information about structural and electronic features of molecules and solids.[1] However, the interpretation of generally complex vibrational spectra usually relies on simulation methods at many different levels of theory. The calculation of vibrational spectra of molecular systems is a well-known procedure, implemented in most of the relevant computer codes.[2,3] The method is based on the calculation of the Hessian matrix, either numerically, from first derivatives,[4] or analytically; the latter is known to be computationally more efficient.[5] The situation is different for crystalline systems, where the development of reliable and accurate computer codes is at an earlier stage than in molecular quantum chemistry and, as a matter of fact, only few *ab initio* codes permit the calculation of vibrational spectra of crystalline compounds. So far, to our knowledge, the most consistent implementations are those employing Density Functional Perturbation Theory methods and using plane waves as a basis set.[6–9] Another widely adopted method of computing vibrational spectra consists simply in Fourier transforming the velocity autocorrelation function derived from a molecular dynamics trajectory.

Our implementation in the periodic *ab initio* CRYSTAL code,[10] that uses a basis of localized functions, is similar to the

Correspondence to: R. Dovesi; e-mail: roberto.dovesi@unito.it

computational scheme of molecular codes. It is based on a recent implementation of analytical energy gradients with respect to the nuclear positions.[11–13] The Hessian matrix at Γ is then obtained from first derivatives by numerical differentiation, as analytical second derivatives are not yet implemented in CRYSTAL.

The effect of hamiltonian, basis set, and numerical parameters of the calculation, including the integration grid in Density Functional Theory (DFT) calculations, has been well documented in the case of small molecules,[14–17] but not in the case of periodic systems, where the algorithms are much less consolidated and a variety of methods have been proposed. The overall accuracy of the proposed computational schemes and computer codes is generally not documented, so that the reason of discrepancies in published data is usually not clear. If this is the case for the lattice parameter of a simple system like MgO, where differences as large as 2% have been obtained with apparently the same hamiltonian and good basis sets,[18,19] *a fortiori* the computational parameters are expected to play a relevant role in the calculation of the more delicate vibrational spectra. Consider, for instance, the vibrational frequencies of α-quartz, calculated by Gonze et al.[7] and by Umari et al.[8] at the same level of theory (DFT-LDA) and using the same plane-wave basis set; differences as large as 64 cm^{-1} are observed, that are attributed by Umari[8] to the different (calculated) equilibrium geometry. The relatively large literature concerning the problem of accuracy in the calculation of vibrational frequencies in molecules, in particular with DFT (grid, rotational invariance, etc.)[16,17,20] and the evidence that even more severe problems are to be expected in the case of periodic systems prompted us to carefully investigate these effects. The evaluation of vibrational frequencies in our scheme involves the calculation of total energy and gradients both for the predetermination of the equilibrium geometry and the very calculation of frequencies. As these are demanding tasks from a computational point of view, a proper setting of the computational parameters must be found that represent a good compromise (if any) between cost and accuracy.

In this work we present a systematic study of the dependence of vibrational spectra on the computational parameters in the CRYSTAL package.[10] We selected α-quartz (SiO_2) as a case study, because it represents a sort of prototype for the very large, important, and extensively investigated family of silicates (including zeolites). Moreover, accurate experimental[21,22] and calculated *ab initio* spectra are available for comparison.[7,8]

The structure of the article is as follows. We first describe the method employed for the calculation of vibrational spectra. The Methodology section describes in short the implementation of the Hartree–Fock (HF) and DFT techniques in the CRYSTAL package, and outlines the parameters that control accuracy. The Results section presents the data concerning the effect of the computational parameters on vibrational spectra of α-quartz, whereas we defer to a forthcoming article the discussion of the basis set effects on a set of various compounds (polymers, slabs, ionic, and covalent crystals). Final comments, including operative conditions for accurate vibrational frequency calculations, are given in the Conclusions.

Basic Equations

Let us summarize the main features of the CRYSTAL program.

Local Orbitals

CRYSTAL uses a basis set of local functions (to be called in the following "Atomic Orbitals," AO), namely, Gaussian Type Functions (GTF):

$$\chi_\mu(\mathbf{r}-\mathbf{G}) = \sum_\alpha d_\mu^\alpha \chi_{\ell m}(\alpha, \mathbf{r}-\mathbf{A}_\mu-\mathbf{G}) = \sum d_\mu^\alpha X_{\ell m}(\mathbf{r}-\mathbf{A}_\mu-\mathbf{G})\exp(-\alpha(\mathbf{r}-\mathbf{A}_\mu-\mathbf{G})^2)$$

defined in the space of coordinates $\mathbf{r}$, where μ labels an AO in the reference (or *zero*) cell, d_μ^α are the contraction coefficients of Gaussian functions with exponent α and centroid $\mathbf{A}_\mu$ in the *zero* cell, $\mathbf{G}$ is a lattice vector locating the AO in the lattice and $X_{\ell m}$ is a real solid spherical harmonic.

Bloch Functions

CRYSTAL is a direct space program, meaning that all the relevant matrices (Fock and overlap) are evaluated in direct space, that is, in the AO basis. A unitary transformation from the AOs to a Bloch function (reciprocal, or $\mathbf{k}$ space) basis

$$\phi_\mu(\mathbf{k}, \mathbf{r}) = \sum_{\mathbf{G}} \exp(i\mathbf{k}\cdot\mathbf{G})\chi_\mu(\mathbf{r}-\mathbf{G})$$

is performed just before the crucial step of diagonalization.

In this basis the Fock (or Kohn–Sham or overlap) matrix has the form:

$$F_{\mu\nu}(\mathbf{k}) = \sum_{\mathbf{G}} \exp(i\mathbf{k}\cdot\mathbf{G})\, F_{\mu\nu}(\mathbf{G})$$

$$F_{\mu\nu}(\mathbf{G}) = T_{\mu\nu}(\mathbf{G}) + C_{\mu\nu}(\mathbf{G}) + X_{\mu\nu}(\mathbf{G})$$

where $F_{\mu\nu}(\mathbf{G})$ is the matrix element corresponding to the interaction between the μ-th AO located in the *zero* cell and the ν-th AO located in the $\mathbf{G}$ cell. The row index can be limited to the *zero* cell for translational invariance, however, the $\mathbf{G}$ summation extends in principle to all direct lattice vectors. T, C, and X are the kinetic, Coulomb, and exchange contributions to the Fock matrix in direct space. Hartree–Fock and Kohn–Sham equations differ in the last term only. Matrices in $\mathbf{k}$ space take a block diagonal form, as Bloch functions are bases for the Irreducible Representations of the Translation Group, each block having the dimension of the AO basis in the unit cell. Fortunately, only a finite and usually small subset of these blocks, corresponding to a suitable sampling of $\mathbf{k}$ points, need to be diagonalised, because interpolation techniques can be used to calculate eigenvalues and eigenvectors in the first Brillouin zone. In CRYSTAL we use a commensurate net[23] that can be specified by a shrinking factor s, that corresponds to the number of intervals in which the reciprocal lattice vectors are divided. The eigenvectors of $F(\mathbf{k})$ are then combined and anti-Fourier transformed to give $P(\mathbf{G})$, the density matrix in direct

space, that is used to build $F(\mathbf{G})$ at the next cycle. The iterative process is stopped as soon as the change in total energy is below a tolerance, t_E. Like all other properties, vibrational spectra obviously depend on s and t_E, as well as on the parameters controlling the accuracy of the Coulomb and exchange infinite series.

Coulomb and Exchange Series

Integrals are evaluated analytically. The Coulomb contribution C (which is the sum of the bielectronic B and nuclear attraction Z terms) to the Fock matrix can formally be written as:

$$C_{\mu\nu}(\mathbf{G}) = B_{\mu\nu}(\mathbf{G}) + Z_{\mu\nu}(\mathbf{G}) =$$

$$= \sum_{\lambda,\rho} \sum_{\mathbf{G}',\mathbf{M}} P_{\lambda\rho}(\mathbf{G}') \int\int \chi_\mu(\mathbf{r}_1)\chi_\nu(\mathbf{r}_1 - \mathbf{G})|\mathbf{r}_1 - \mathbf{r}_2|^{-1}\chi_\lambda(\mathbf{r}_2 - \mathbf{M}) \times \chi_\rho(\mathbf{r}_2 - \mathbf{M} - \mathbf{G}')d\mathbf{r}_1 d\mathbf{r}_2 +$$

$$- \sum_{\mathbf{M}} \sum_{A} \int \chi_\mu(\mathbf{r}_1)\chi_\nu(\mathbf{r}_1 - \mathbf{G})|\mathbf{r}_1 - \mathbf{M} - \mathbf{A}|^{-1} N_A d\mathbf{r}_1 \quad (1)$$

where the summations on μ, ν, ρ, and λ extend to the AOs in the unit cell; $\mathbf{G}$, $\mathbf{G}'$, and $\mathbf{M}$ extend in principle to all the (infinite) lattice vectors, and N_A is the nuclear charge of atom A.

It is clear that the treatment of the Coulomb term, as containing three infinite lattice summations, requires a careful analysis and some engineering to ensure high numerical accuracy and computational efficiency. We refer to a previous and probably not widely known article[24] for an exhaustive discussion of the Coulomb problem with infinite three-dimensional systems and of the algorithms implemented in CRYSTAL. Here we provide an overview of the guidelines adopted in CRYSTAL for the treatment of the infinite series. These are based on three simple observations:

- The overlap between two GTFs decays exponentially with distance. This property can be exploited for the selection of a set of $\mathbf{G}$ and $\mathbf{G}'$ in the Coulomb term above. We proceed as follows: a single normalized s-type Gaussian is associated with each atomic shell (adjoined Gaussian); the calculation of the integrals between the AOs belonging to the two shells is avoided if the overlap is smaller than $10^{-\mathrm{ITOL1}}$, where ITOL1 is one of the input parameters. A similar criterion applies to two of three sums in the exchange series (see below).
- The electrostatic potential generated by a charge distribution at a nonoverlapping point can be approximated by a (truncated) multipolar expansion of the charge distribution. Speed of convergence and truncation criteria of the expansion depend on the distance between the target point and the charge distribution, the position of the expansion center, size and shape of the charge distribution. Let us define a partition of the cell charge distribution, for example, in terms of Mulliken atomic charges ρ_A:

$$\rho(\mathbf{r}) = \sum_{A} \sum_{\mathbf{M}} \rho_A(\mathbf{r} - \mathbf{A} - \mathbf{M})$$

where

$$\rho_A(\mathbf{r} - \mathbf{A}) = \sum_{\lambda \in A} \sum_{\rho} \sum_{\mathbf{G}'} P_{\lambda\rho}(\mathbf{G}')\chi_\lambda(\mathbf{r})\chi_\rho(\mathbf{r} - \mathbf{G}') - N_A\delta(\mathbf{r} - \mathbf{A})$$

is translation invariant and the last term is the nuclear charge contribution. Equation (1) can then be rewritten as:

$$C_{\mu\nu}(\mathbf{G}) = \sum_{A} \sum_{\mathbf{M}} \int\int \rho_{\mu\nu}(\mathbf{r}_1 - \mathbf{G})|\mathbf{r}_1 - \mathbf{r}_2|^{-1} \times \rho_A(\mathbf{r}_2 - \mathbf{A} - \mathbf{M})d\mathbf{r}_1 d\mathbf{r}_2 \quad (2)$$

with

$$\rho_{\mu\nu}(\mathbf{r}_1 - \mathbf{G}) = \chi_\mu(\mathbf{r}_1)\chi_\nu(\mathbf{r}_1 - \mathbf{G})$$

If the overlap between charge distributions ρ_A and $\rho_{\mu\nu}$ (again evaluated by using the "adjoined Gaussian") is smaller than a given threshold ($10^{-\mathrm{ITOL2}}$) for any $\mathbf{M}$, eq. (2) is approximated as follows (L is the maximum order of the multipolar expansion):

$$C_{\mu\nu}(\mathbf{G}) = \sum_{A} \sum_{\ell m}^{L} \left(\sum_{\mathbf{M}} \gamma_{\ell \mathrm{m}}(\mathrm{A})\Phi_{\mu\nu\ell \mathrm{m}}(\mathbf{G}, \mathbf{A} + \mathbf{M}) \right) \quad (3)$$

so that $C_{\mu\nu}$ is expressed in terms of the multipole moments of ρ_A ($N_{\ell m}$ is a normalization factor)

$$\gamma_{\ell m}(A) = N_{\ell m} \int \rho_A(\mathbf{r}_2 - \mathbf{A})X_{\ell m}(\mathbf{r}_2 - \mathbf{A})d\mathbf{r}_2$$

and of the field integrals

$$\Phi_{\mu\nu\ell m}(\mathbf{G}, \mathbf{A} + \mathbf{M}) = \int \chi_\mu(\mathbf{r}_1)\chi_\nu(\mathbf{r}_1 - \mathbf{G}) \times X_{\ell m}(\mathbf{r}_1 - \mathbf{A} - \mathbf{M})|\mathbf{r}_1 - \mathbf{A} - \mathbf{M}|^{-2\ell - 1}d\mathbf{r}_1$$

The infinite summation on $\mathbf{M}$ can be performed by using the Ewald technique, which reduces it to a finite number of terms.[24]

Thus, three parameters, ITOL1, ITOL2, and L, control the accuracy of the Coulomb series.

- The density matrix decays with distance from the diagonal. In a localized basis set, the elements of the density matrix of an insulator decay exponentially with the distance between centers; the larger the gap, the faster the decay. Density matrix in direct space decays to zero with distance for conductors, too, but much more slowly.[25,26] This behavior is exploited for an efficient truncation of the exchange series in the Fock matrix expression:

$$X_{\mu\nu}(\mathbf{G}) = \sum_{\lambda,\rho} \sum_{\mathbf{G}'} P_{\lambda\rho}(\mathbf{G}') \times \sum_{\mathbf{M}} \int\int \chi_\mu(\mathbf{r}_1)\chi_\lambda(\mathbf{r}_1 - \mathbf{M})|\mathbf{r}_1 - \mathbf{r}_2|^{-1} \times \chi_\nu(\mathbf{r}_2 - \mathbf{G})\chi_\rho(\mathbf{r}_2 - \mathbf{M} - \mathbf{G}')d\mathbf{r}_1 d\mathbf{r}_2 \quad (4)$$

The above equation shows that the $\mathbf{M}$ summation is limited by the exponential decay of the product $\chi_\mu^{\mathbf{0}}\chi_\lambda^{\mathbf{M}}$. This condition and the

decay of the product $\chi_\nu^{\mathbf{G}}\chi_\rho^{\mathbf{M}+G'}$ limit the difference between the moduli of the **G** and **G′** vectors; a parameter ITOL3 (having the same meaning as ITOL1 used for the Coulomb series) is used to truncate the two summations every time the difference between **G** and **G′** is large, although their moduli may individually be large. However, the exponential decay of the density matrix permits us to disregard integrals involving **G** (ITOL4) and **G′** (ITOL5) vectors with large moduli. The exchange series is then truncated according to these criteria, where long-range effects are not taken into account, as they are expected to be negligible (see ref. 25 for more details). The truncation criteria just described are crucial in determining both accuracy and cost of the calculation.

DFT Grid

DFT schemes rely on numerical integration for the evaluation of the contribution of the exchange-correlation functional and its gradients. The generation of grid points in CRYSTAL is based on an atomic partition method, originally developed by Becke[27] for molecular systems and then extended to periodic systems.[28] In this scheme the integration volume V_{cell} (cell volume) of a function $f(\mathbf{r})$ is partitioned into atomic volumes, each centered at nucleus A and associated with weight $w_A(\mathbf{r})$. Spherical coordinates are introduced to separate radial and angular integration

$$\int_{V_{\text{cell}}} f(\mathbf{r})d\mathbf{r} = \sum_A \int_0^\infty dr_A r_A^2 \int_0^{4\pi} d\Omega w_A(r_A, \Omega_A) f(r_A, \Omega_A) \cong \sum_A \sum_{i,j} r_{Ai}^2 w(r_{Ai}, \Omega_{Aj}) f(r_{Ai}, \Omega_{Aj}),$$

Here, the sums on A extend to all nuclei in the zero cell and $r_A = |\mathbf{r} - \mathbf{R}_A|$ is the distance of a point in the cell from nucleus A, Ω is the solid angle. In CRYSTAL, radial and angular points of the grid are generated through Gauss–Legendre and Lebedev quadrature schemes. For details about the implementation of DFT in CRYSTAL03, the actual expressions for $f(\mathbf{r})$, and the calculation of electron density, see ref. 29. The grid size has a strong impact on both accuracy and cost of the calculation. Therefore, tuning the grid is important to ensure numerical stability while keeping the cost of the calculation affordable. One possible strategy is called grid pruning, and is based on the observations that the electron density at short radii has essentially spherical symmetry and that, far from nuclei, weights $w(r_{Ai}, \Omega_{Aj})$ are relatively small. Accordingly, the angular quadrature in pruned grids is not radially uniform, that is, index j of the sum in the right member of eq. (5) varies with i. In particular, the number of angular points is maximum in the valence region and decreases gradually out of it in both directions. If properly designed, a pruned grid is expected to be about as accurate as the corresponding unpruned grid and much more efficient.

The Analytical Gradient

The analytical gradients of energy with respect to the atomic fractional coordinates have been evaluated as discussed in refs. 11–13 for HF and in ref. 29 for DFT and hybrid functionals. The same truncation criteria adopted for the calculation of the Fock matrix elements and the energy have been used also for gradients.

The Optimizer and the Related Parameters

Energy gradients allow automatic search for equilibrium nuclear positions using a modified conjugate gradient algorithm as proposed by Schlegel.[30] The actual implementation of the automated geometry optimisation in CRYSTAL03 has recently been described,[31] showing that geometry optimisation is now feasible for molecules, polymers, slabs, and crystals. Geometry optimisation is performed in cartesian coordinates. At each step the gradients and the estimated nuclear displacements for the next step are evaluated, and convergence is tested with reference to the root-mean-square value of both the gradients (G_{rms}) and the estimated nuclear displacements (X_{rms}) as well as on the absolute value of their largest component, denoted as $G_{\max}$ and $X_{\max}$, respectively. Optimisation is considered as complete when the values of these four parameters are all simultaneously below certain thresholds.

Calculation of Vibrational Spectra

We shall begin our analysis from the molecular case and then add a few remarks about the treatment of systems periodic in one, two, and three dimensions.

Born–Oppenheimer potential energy surface of a system with N nuclei, $V(\mathbf{x})$, is a function of vector $\mathbf{x}$ of the $3N$ coordinates of the atoms in a system. In the harmonic approximation, it takes the form:

$$V(0) = \frac{1}{2}\sum_{ij} u_i H_{ij} u_j \equiv \frac{1}{2}\langle u|H|u\rangle$$

where u_i represents a displacement of the i-th cartesian coordinate from its equilibrium value, H is the Hessian matrix of the second derivatives of $V(\mathbf{x})$, evaluated at equilibrium, with respect to the displacement coordinates

$$H_{ij} = \frac{1}{2}\left[\frac{\partial^2 V(\mathbf{x})}{\partial u_i \partial u_j}\right]_0$$

and the usual bra and ket notation is used for row and column representation of the $3N$-component vector. In terms of the weighted displacement coordinates $q_i = \sqrt{M_i}u_i$, where M_i is the mass of the atom associated with the i-th coordinate, the classical vibrational Hamiltonian of a polyatomic molecule becomes:

$$\mathcal{H} = T + V = \frac{1}{2}\left(\sum_i M_i \dot{u}_i^2 + \sum_{ij} u_i H_{ij} u_j\right) + V_0 = \frac{1}{2}\left(\langle p|p\rangle + \langle q|W|q\rangle\right) + V_0 \quad (6)$$

where $p_i = \dot{q}_i$, V_0 is the electron potential and

$$W_{ij} = H_{ij}/\sqrt{M_i M_j}$$

is the weighted Hessian. The eigenvalues κ_j of the hermitian matrix W are the generalized force constants. Equation (6) can then be factorized into $3N$ one-dimensional harmonic problems:

$$\mathcal{H} = \sum_v h_v = \sum_v \frac{1}{2}(P_v^2 + \omega_v^2 Q_v^2))$$

From this point of view, each of the $3N - 6$ vibrational modes can be seen as a collective oscillatory motion with frequency $\omega_v = \sqrt{\kappa_j}/2\pi$.

Following the approach just described, the problem of calculating vibrational spectra reduces to the diagonalization of W to find the set of eigenvalues κ_j.

In CRYSTAL, energy first derivatives with respect to the atomic positions, $v_j = \partial V/\partial u_j$, are calculated analytically[11–13,29] for all u_j coordinates, while second derivatives at $\mathbf{u} = 0$ (where all first derivatives are zero) are calculated numerically using a "two-point" formula ($N = 2$)

$$\left[\frac{\partial v_j}{\partial u_i}\right]_0 \approx \frac{v_j(0, \ldots, u_i, 0, \cdots)}{u_i} \tag{7}$$

or a "three-point" formula ($N = 3$) to improve the numerical calculation of second derivatives:

$$\left[\frac{\partial v_j}{\partial u_i}\right]_0 \approx \frac{v_j(0, \ldots, u_i, 0, \cdots) - v_j(0, \ldots, -u_i, 0, \cdots)}{2u_i} \tag{8}$$

Because $v(u_1, \ldots, u_{3N})$ has the full symmetry of the crystal, simplification of the algorithm is possible in two respects:[4] (1) reduce the explicit calculation of the derivatives to a minimal set, and (2) factorize the W matrix before diagonalization.

Two parameters control the numerical calculation of W in CRYSTAL: the increment given to each cartesian atomic coordinate (u), and the number of points ($N = 2, 3$) used in evaluating second derivatives [eqs. (7) and (8)].

For an infinite periodic system, the molecular approach needs modification with respect to two important points (we refer to Born–Huang[32] for further details or to any standard introduction to the subject, see, e.g., ref. 33):

1. The infinite nature of the crystalline system imposes the use of translational invariance to keep the size of matrices finite. This corresponds to using the basis of the generalized coordinates $q_i(\mathbf{k})$, instead of the q_i coordinates defined above

$$q_i(\mathbf{k}) = N \sum_G \exp[-i\mathbf{k}\cdot\mathbf{G}] q_i^{\mathbf{G}}$$

and permits to block-factorize the vibrational problem into a set of problems (one for each $\mathbf{k}$ point in the Brillouin zone) of dimension $3N$, where N is the number of atoms in the unit cell. The $\mathbf{k}$-th block of the $\mathbf{k}$-factorized W matrix takes the form:

$$W_{ij}(\mathbf{k}) = \sum_{\mathbf{G}} \exp[i\mathbf{k}\cdot\mathbf{G}] \frac{H_{ij}^{0G}}{\sqrt{M_i M_j}}$$

where H_{ij}^{0G} is the second derivative of $V(\mathbf{x})$ at equilibrium with respect to atom i in cell $\mathbf{0}$ (translation invariance is exploited) and atom j in cell $\mathbf{G}$. In the following we will only consider the special point $\Gamma = (0, 0, 0)$, where the above equation reduces to

$$W_{ij}(0) = \sum_{\mathbf{G}} \frac{H_{ij}^{0G}}{\sqrt{M_i M_j}} \tag{9}$$

Frequencies at Γ are evaluated exactly in the same way as described for molecules: a set of $(3N + 1)$ SCF calculations of the unit cell are performed at the equilibrium geometry and incrementing each of the $3N$ nuclear coordinates in turn by u (use of symmetry can reduce the number of the required calculations drastically). Second-order energy derivatives are evaluated according to eq. (7). Obtaining frequencies at $\mathbf{k}$ points different from Γ would imply the construction of appropriate supercells. As anticipated above, we will limit our analysis to the Γ point frequencies, because: (a) this is enough for exploring the numerical effects we are interested in in this article (the accuracy attained with CRYSTAL for supercells of various size is the same); (b) dispersion effects are relatively small in this case; (c) RAMAN and infrared experimental data,[21,22] as well as previous calculations,[7,8] refer to the Γ point only.

2. In the case of ionic compounds, long-range Coulomb effects due to coherent displacement of the crystal nuclei are neglected, as a consequence of imposing the periodic boundary conditions (see sections 5, 10, 34, and 35 in ref. 32). Therefore, $W_{ij}(\mathbf{0})$ needs to be corrected for obtaining the longitudinal optical (LO) modes [eqs. (3) and (6) in ref. 8]. This additional term essentially depends on (a) the electronic (clamped nuclei) dielectric tensor ε^{∞}, and (b) the *Born effective charge tensor* associated to atom A: $\mathbf{Z}^{A*}$ which have been shown[34–36] to be quite stable with respect to the computational parameters we are discussing in this article. For this reason, and for conciseness, we will limit the following discussion to the Transverse Optical (TO) part of the α-quartz spectrum.

Results

Vibrational spectra of α-quartz have been calculated with different settings of the computational parameters illustrated in the previous section in order to check their influence on results. In summary, these parameters can be classified into three groups:

1. Parameters controlling accuracy in a single energy point calculation:
   (a) convergence criteria of the Coulomb and exchange infinite summations in Fock matrix definition [eqs. (1), (3), and (4)] and of the total energy. The current implementation of CRYSTAL allows simultaneous control over all five threshold values [ITOL1 ITOL2 ITOL3 ITOL4 ITOL5] through the keyword TOLINTEG. In this work, we have studied the dependence of vibrational spectra on the truncation criteria by testing three different sets of threshold values denoted as $t_{\text{int}} = 1, 2, 3$ and corresponding to [6 6 6 6 12], [7 7 7 7 14], and [8 8 8 8 16], respectively. If not otherwise specified, default is $t_{\text{int}} = 1$. The depen-

Table 1. Dependence of HF Equilibrium Geometry and Vibrational Frequencies of α-Quartz at Γ on Different Truncation Levels (t_{int} Parameter, see Text for Definition) of the Coulomb and Exchange Series.

t_{int}	1	2	3
a	4.965414	4.961913	4.961191
c	5.440650	5.446365	5.448669
Si_x	0.471915	0.471934	0.472250
O_x	0.416530	0.416340	0.416265
O_y	0.264163	0.263867	0.263525
O_z	0.122738	0.122986	0.123150
Si_1—O	1.6133	1.6125	1.6124
Si_2—O	1.6159	1.6160	1.6158
Si—O—Si	145.51	145.55	145.58
$\overline{\lvert\Delta\rvert}$	1.2	0.6	0.0
Δ_{min}	−3.7	−1.1	0.0
Δ_{max}	2.8	1.6	0.0

a and c are the lattice parameters (in Å); Si_x, O_x, O_y, and O_z denote the fractional coordinates of silicon and oxygen atoms in the asymmetric unit cell; Si—O distance is in Å and the angle Si—O—Si in degrees. $\overline{\lvert\Delta\rvert}$, Δ_{min}, Δ_{max} (see text for definitions) are all referred to the frequencies ω_v^{ref} computed with $t_{\text{int}} = 3$.

dence of accuracy in vibrational spectra on L (multipole moment order) in eq. (3) has also been investigated, the default setting being $L = 4$.

(b) The number of radial (n_r) and angular (n_Ω) points of the grid used for numerical integration of $f(\mathbf{r})$ [eq. (5)] in DFT calculations. In this study we have tested several grids, which will be referred to with the notation (n_r, n_Ω). In CRYSTAL, all the grid points associated with very small weights w are discarded (if smaller than $1 \cdot 10^{-14}$ in the present calculations), so that the total number of points n_p is usually smaller than $n_r \times n_\Omega$. Symbol (n_r, n_Ω)p labels a pruned grid with n_Ω points on Lebedev surfaces in the most accurate integration region.

(c) The SCF total energy convergence criteria t_E. The SCF cycle stops when the energy difference (absolute value) from the previous cycle is smaller than $1 \cdot 10^{-t_E}$ hartree. Default value is $t_E = 9$.

(d) The shrinking factor for the definition of the reciprocal lattice grid. Default value is $s = 3$, corresponding to seven **k** points in the asymmetric Brillouin zone.

2. Parameters controlling convergence to the equilibrium geometry during optimizations. In CRYSTAL03, the GTOL and XTOL parameters are the thresholds for G_{rms} and X_{rms}. The corresponding thresholds for G_{max} and X_{max} are defined as 1.5 times GTOL and XTOL, respectively. Default values are GTOL $= 3 \cdot 10^{-4}$ a.u. and XTOL $= 1.2 \cdot 10^{-3}$ bohr.
3. Parameters controlling the numerical estimate of energy second derivatives with respect to the atomic coordinates, such as

(a) the finite displacement used for evaluating the derivative numerically [eqs. (7) and (8)]. Default value is $u = 0.001$ bohr.

(b) the formula adopted for the evaluation of the derivative. The default here adopted is $N = 2$, corresponding to using eq. (7).

The first part of this section refers to HF results; then our analysis is extended to DFT in the Local Density Approximation (LDA).[37,38] Regarding basis sets, modified 6-21G* and the 6-31G* for Si and O, respectively, have been used, the exponents of the most diffuse sp and d orbitals being (0.13, 0.5) for Si and (0.274, 0.6) for O.

Our analysis begins by exploring the influence of the computational parameters (t_{int} and L) controlling accuracy of the Coulomb and exchange series on vibrational frequencies in the HF approximation. Results are summarized in Table 1. The three columns refer to calculations performed with $t_{\text{int}} = 1, 2, 3$, at the corresponding equilibrium geometry. The three predicted geometries are extremely similar, as the Si—O distance changes by less than 0.001 Å and the Si—O—Si angle by less than 0.1 degrees. The variability of the calculated frequencies ω_v of the M ($M = 24$) TO vibrational modes is estimated through three global indices with reference to the set of ω_v^{ref} reported in the first column of Table 2, which have been obtained with the most accurate t_{int} used ($t_{\text{int}} = 3$). Our indices are defined as follows (in units of cm^{-1}):

$$\overline{\lvert\Delta\rvert} = \sum_{v=1}^{M} |\omega_v - \omega_v^{\text{ref}}|/M$$

$$\begin{aligned} \Delta_{\text{max}} &= \max(\omega_v - \omega_v^{\text{ref}}) \\ \Delta_{\text{min}} &= \min(\omega_v - \omega_v^{\text{ref}}) \end{aligned} \qquad v = 1, 2, \ldots, M$$

Table 2. Calculated and Experimental Vibrational Frequencies (cm^{-1}) of α-Quartz at Γ.

Symmetry	HF[a]	LDA[a]	LDA[b]	LDA[c]	Exp.[d]
A_1	202.5	254.5	193.7	238.9	219
	376.2	317.3	355.0	339.3	358
	498.0	471.0	460.1	461.7	469
	1145.7	1077.1	1123.3	1061.0	1082
A_{2T}	396.3	321.7	366.4	341.3	361.3
	530.9	487.4	489.3	493.4	499
	820.6	775.9	792.2	762.4	778
	1137.5	1074.4	1115.4	1056.5	1072
E_T	136.3	134.5	120.9	133.3	133
	280.6	255.2	257.3	261.3	269
	425.7	365.8	390.0	377.6	393.5
	485.0	431.5	448.0	443.8	452.5
	731.8	707.7	703.3	690.8	698
	834.2	816.2	809.6	791.7	799
	1131.2	1059.3	1108.7	1045.0	1066
	1238.5	1129.7	1190.8	1128.1	1158

HF and LDA data in the present work have been calculated with $t_{\text{int}} = 3$ and the (55, 974) grid, respectively.
[a]Present work.
[b]Ref. 8.
[c]Ref. 7.
[d]Ref. 21.

Table 3. Dependence of HF Vibrational Frequencies of α-Quartz at Γ on L [the Multipole Order in eq. (3)], t_E (SCF Convergence Tolerance), s (the Shrinking Factor Used in the Brillouin Zone), u (Displacement in the Numerical Evaluation of the Hessian from the Analytical Energy Gradients), and N (Number of Total Energy Calculations along Each Nuclear Cartesian Coordinate for the Evaluation of the Hessian Matrix).

		$\overline{\lvert\Delta\rvert}$	Δ_{min}	Δ_{max}
L	2	5.6	−10.1	12.3
	4	0.5	−1.4	1.2
	8	1.9	−4.9	−0.2
t_E	9	0.5	−1.6	0.0
	10	0.1	−0.3	0.0
s	3	0.0	0.0	0.0
	0.01	2.2	−6.3	0.0
u	0.005	0.9	−2.7	0.0
	0.002	0.2	−0.6	0.0
	0.0005	0.2	0.0	0.4
N	2	0.3	−0.7	0.0

$\overline{\lvert\Delta\rvert}$, Δ_{min}, Δ_{max} (see Table 1) are computed with respect to the frequencies evaluated with $L = 6$, $t_E = 11$, $s = 6$, $u = 0.001$ bohr and $N = 3$, respectively.

The three settings provide frequency values (Table 1) in good agreement with each other, the largest difference being 3.7 cm^{-1} with $t_{int} = 1$ and decreasing to 1.6 cm^{-1} with $t_{int} = 2$. $\overline{\lvert\Delta\rvert}$ is small in both cases (1.2 and 0.6 cm^{-1}). If the calculation of vibrational frequencies with different t_{int} is performed at the same geometry, for example the $t_{int} = 1$ equilibrium geometry, the largest difference in frequencies reduces to 1.9 and 1.4 with $t_{int} = 1$ and $t_{int} = 2$, showing that the change in equilibrium geometry is still slightly appreciable in the first case, but becomes negligible in the latter case, where the equilibrium geometry is nearly indistinguishable from that obtained with the reference setting ($t_{int} = 3$). The cost of both optimization and frequency calculation for $t_{int} = 1$, 2, and 3 scales roughly as 1.0:1.6:2.6.

Regarding the influence of different choices of L [eq. (3)] on vibrational spectra, Table 3 shows that $L = 4$ is a suitable choice, $\overline{\lvert\Delta\rvert}$ being very small, whereas accuracy would still be slightly unsatisfactory with $L = 2$.

The calculation of very accurate analytical gradients, as is needed for the numerical evaluation of vibrational frequencies, requires that the SCF cycle be very well converged. The results obtained for convergence on the total energy within $t_E = 8, 9, 10$ are reported in Table 3 with reference to the very well converged data corresponding to $t_E = 11$. At $t_E = 8$, $\overline{\lvert\Delta\rvert}$ is 1.9 cm^{-1} with a maximum difference in the calculated frequency values of 4.9 cm^{-1}; at $t_E = 9$, $\overline{\lvert\Delta\rvert}$ reduces to only 0.5 cm^{-1}, and the largest difference is only 1.6 cm^{-1}. At $t_E = 10$, $\overline{\lvert\Delta\rvert}$, Δ_{min} and Δ_{max} all become negligible.

The test on the shrinking factor s confirms that $s = 3$ is absolutely correct, as the frequency values in this case show no appreciable difference from $s = 6$, corresponding to 34 **k** points in the asymmetric Brillouin zone.

Table 3 also provides information on the importance of the u parameter [see point 3(a) at the beginning of this section]. HF frequencies have been calculated with steps $u = 0.0005$, 0.001, 0.002, 0.005, 0.01 Å along each nuclear cartesian coordinate. The reference case is the default value in CRYSTAL (0.001 Å). Steps in the 0.0005–0.005 Å range produce frequencies that differ by at most 2.7 cm^{-1}. In the 0.0005–0.002 Å range of u, frequencies are fairly stable, with the maximum difference smaller than 1 cm^{-1}, although the corresponding variation in energy is in the order of 1, 0.1, 0.01 μhartree for $u = 0.002$, 0.001, 0.0005 Å, respectively, confirming that very accurate energy calculations are necessary for accurate numerical evaluation of second order energy derivatives.

The last parameter we want to discuss here is N [see point 3(b) at the beginning of this section]. Table 3 shows that the frequencies obtained with $N = 2$, referred to the more accurate $N = 3$ formula, correspond to very small $\overline{\lvert\Delta\rvert}$, Δ_{min} and Δ_{max}, the largest difference being 0.7 cm^{-1}. Therefore, as a rule, we will use $N = 2$, even if slightly less accurate, because this corresponds to reducing the cost of the calculation by a factor 2.

Another point to be considered is how accurate the determination of the equilibrium geometry must be in the calculation of vibrational frequencies. First, we consider the optimization of fractional coordinates in the unit cell at the equilibrium cell volume. In Table 4, the quality of the vibrational frequencies obtained at different levels of approximation of the equilibrium nuclear positions is examined. Decreasing values of G_{rms} and G_{max} from case 1 to 4 in the table correspond to progressively approaching the "true" minimum energy structure with the default setting of the computational parameters. In case 2, where G_{rms} and G_{max} still exceed the default thresholds in CRYSTAL03 (GTOL), the maximum difference in frequencies from case 4 is already below 2 cm^{-1} and $\overline{\lvert\Delta\rvert}$ is less than 1 cm^{-1}, whereas case 3 essentially coincides with case 4. Cases 1–4 are actually steps of a real geometry optimization process with the default values of GTOL and XTOL, predicting case 3 as the resulting optimized geometry.

Table 4. Dependence of the HF Vibrational Coordinates of α-Quartz at Γ on the Unit Cell Internal Geometry with $a = 4.965414$ Å and $c = 5.440650$ Å.

Case	1	2	3	4
Si_x	0.469300	0.471880	0.471955	0.471944
O_x	0.417994	0.416479	0.416504	0.416506
O_y	0.268784	0.263759	0.263989	0.264012
O_z	0.120052	0.123224	0.122892	0.122875
Si_1—O	1.6164	1.6126	1.6131	1.6131
Si_2—O	1.6196	1.6154	1.6157	1.6158
Si—O—Si	144.95	145.64	145.55	145.55
G_{rms}	0.002011	0.000387	0.000012	0.000002
G_{max}	0.002724	0.000666	0.000018	0.000003
$\overline{\lvert\Delta\rvert}$	7.3	0.8	0.0	0.0
Δ_{min}	−18.8	−1.6	0.0	0.0
Δ_{max}	17.2	1.8	0.1	0.0

Symbols and units as in Table 1. Cases 1 to 4 correspond to improving accuracy in the determination of the equilibrium geometry as measured by the decreasing values of G_{rms} and G_{max} (see text for definition). $\overline{\lvert\Delta\rvert}$, Δ_{min}, Δ_{max} are calculated with reference to case 4.

Table 5. Influence of the Cell Volume on the Vibrational Frequencies of α-Quartz at Γ.

	0.97 V_0	0.99 V_0	V_0	1.01 V_0	1.03 V_0
Volume	112.6845	115.0078	116.1696	117.33127	119.6546
a	4.906132	4.942932	4.965414	4.979869	5.014580
c	5.405738	5.435352	5.440650	5.463202	5.494521
Si_x	0.466710	0.470136	0.471915	0.473778	0.477751
O_x	0.414095	0.415730	0.416530	0.417411	0.418711
O_y	0.272890	0.267319	0.264163	0.261266	0.254088
O_z	0.115909	0.120346	0.122738	0.125185	0.131156
Si_1—O	1.6116	1.6129	1.6133	1.6139	1.6148
Si_2—O	1.6151	1.6157	1.6159	1.6164	1.6167
Si—O—Si	142.7	144.5	145.5	146.5	148.6
ΔE	0.551	0.050	0.000	0.061	0.526
$\lvert\bar{\Delta}\rvert$	10.9	3.5		3.7	11.6
Δ_{min}	−6.4	−2.5		−10.8	−39.0
Δ_{max}	32.5	11.6		2.4	8.4

Optimization of cell parameters and fractional coordinates have been performed at 0.97, 0.99, 1.01, and 1.03 V_0 (the equilibrium volume). ΔE is the difference in total energy (mhartree) with respect to V_0. Symbols and units as in Table 1.

Therefore, default GTOL and XTOL can be accounted very accurate to our purpose.

We can now consider the importance of an accurate definition of the equilibrium a and c lattice parameters. As the energy surface of quartz along a and c is quite flat, small energy differences imply relatively large differences in the lattice parameters, so that precise location of the minimum may be difficult. We performed four additional geometry optimizations at $\pm 1\%$ and $\pm 3\%$ of the equilibrium volume V_0 and computed frequencies. The results are reported in Table 5. Because the expected range of uncertainty in the determination of V_0 with our default computational conditions is smaller than $\pm 1\%$, we first observe that for cell volume variations of 1% in either direction, which correspond to an energy change ΔE of only 0.05 mhartree, $\overline{|\Delta|}$ is about 3.6 cm^{-1}, with a maximum shift of about 11 cm^{-1}. The overall accuracy of our method and its reliability in describing the evolution of frequencies as a function of volume can be checked by considering the whole set of data reported in Table 5 in an energy range of about 0.5 mhartree. The variation of the vibrational frequencies with volume is quite regular, as shown in Figure 1 for the three modes with the largest excursion in the 0.97–1.03 V_0 range (396.3, 530.9 and 1131.2 cm^{-1}, respectively). Such accuracy is fundamental for careful investigation of the effect of pressure on the vibrational spectrum of crystalline compounds and for representing each mode analytically as a function of pressure, in terms of which thermodynamic functions of temperature and volume (or pressure) can be evaluated conveniently.

We now consider DFT calculations within the Local Density Approximation (LDA) using Dirac–Slater[38] exchange and Vosko-Wilk-Nusair[39] correlation potentials. In Table 6 we explore the dependence of frequencies on the grid adopted for the numerical integration. All data are evaluated with reference to a very accurate unpruned grid, (75,5800). The atomic fractional coordinates have been reoptimized for each specific grid, whereas a and c cell parameters have been obtained with the reference grid. The radial and angular components of grids have been examined separately. The first series of data in Table 6 concern the evaluation of unpruned grids with different n_r and constant $n_\Omega = 11$. It is clear that $n_r > 55$ corresponds to no further improvement in accuracy. The second series of data show the dependence of results on n_Ω, when $n_r = 55$. As n_Ω increases, the calculated frequencies approach the reference case more and more closely and the results obtained with the (55, 974) grid can be considered as very well converged. Grid pruning has been tested for the (55, 434) and the (55, 974) grids as examples. It appears as being very effective, the number of points reducing dramatically, from 169,062 points to 58,140 in the first case and from 374,608 to 188,154 in the other

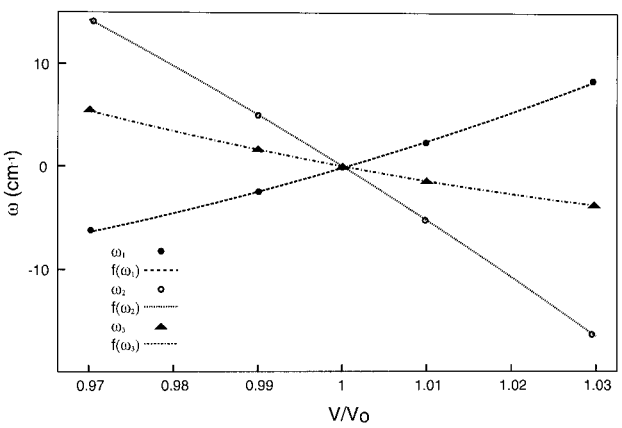

Figure 1. Dependence of vibrational frequencies of α-quartz at Γ on the cell volume V. Three vibrational mode frequencies of A_2 symmetry are represented with their quadratic fitting curves. Frequencies are referred to the respective values at the equilibrium cell volume V_0: $\omega_1 = 396.3$ cm^{-1}, $\omega_2 = 530.9$ cm^{-1}, $\omega_3 = 1131.2$ cm^{-1}.

case, while the results are completely unaffected with respect to those computed with the corresponding unpruned grids.

The availability of results from experimental measurements[21,22] and other theoretical calculations[7,8] for α-quartz has already been mentioned. These and the HF and LDA vibrational frequencies of the present work are reported in Table 2. Table 7, which is aimed to help in the evaluation of these different sets of data, shows that they are much more sparse than in our tests on computational parameters in a range of reasonable accuracy. As expected, HF performs more poorly than LDA, the average disagreement with experiment being $\overline{|\Delta|} = 37\ \mathrm{cm}^{-1}$, and the experimental frequencies are generally overestimated ($\Delta_{\min} = -16$ samples the only mode with lower frequency). LDA results show a less clear trend but better agreement with the experimental data ($\overline{|\Delta|}$ in the range of 13–17 cm^{-1}). However, the agreement with each other of the calculated LDA sets is not as good, the maximum difference observed being even as large as $\Delta_{\max} = 64\ \mathrm{cm}^{-1}$. Moreover, the difference between the results reported in refs. 7 and 8, which were obtained with very similar methods (both for the determination of the wave function and for the calculation of frequencies), is surprisingly larger than the difference between the present results, which have been obtained with a different method, and those in ref. 7. It has been claimed that this may be due to different accuracy in the evaluation of equilibrium geometry.[8] Perhaps basis set effects are also important and deserve investigation. One must also be aware that the comparison of the calculated harmonic and experimental frequencies is not fully appropriate, as these two quantities differ by anharmonic corrections. The real amount of such correction is, at this stage, not easily estimated for solids of relatively large unit cell like quartz (see ref. 6, p. 555).

Table 6. Dependence of the LDA Vibrational Frequencies of α-Quartz at Γ on the Integration Grid.

Grid	n_p	$\overline{\lvert\Delta\rvert}$	$\Delta_{\min}$	$\Delta_{\max}$
(35,302)	75,778	3.7	−8.1	2.0
(45,302)	97,850	2.5	−6.2	2.6
(55,302)	118,106	1.7	−3.9	3.7
(65,302)	139,262	1.7	−3.9	3.8
(75,302)	161,120	1.7	−3.9	3.9
(55,302)	118,106	1.7	−3.9	3.7
(55,350)	136,539	0.8	−1.7	1.1
(55,434)	169,062	1.3	−2.1	3.8
(55,590)	227,788	0.7	−1.3	2.7
(55,770)	296,686	0.7	−1.2	2.9
(55,974)	374,608	0.3	−0.6	0.6
(55,1202)	461,508	0.4	−0.5	0.7
(55,434)*p*	58,140	1.3	−1.5	3.7
(55,974)*p*	188,154	0.4	−0.7	0.7

n_p denotes the total number of points in an unpruned grid originated from (n_r, n_Ω) radial and angular quadratures. Symbol $(n_r, n_\Omega)p$ denotes pruned grids. All other symbols and units as in Table 1. $\overline{|\Delta|}$, $\Delta_{\min}$, $\Delta_{\max}$ are referred to the limiting case of a very dense grid, (75, 5810), with $n_p = 3 \cdot 10^6$.

Table 7. Comparison through $\overline{|\Delta|}$, $\Delta_{\min}$, and $\Delta_{\max}$ (cm^{-1}) of the Different Sets of Calculated and Experimental Vibrational Frequencies of α-Quartz at Γ Reported in Table 2.

		LDA[a]	LDA[b]	LDA[c]	Exp.[d]
	HF[a]	48	28	50	37
$\overline{\lvert\Delta\rvert}$	LDA[a]		26	12	16
	LDA[b]			26	17
	LDA[c]				13
	HF[a]	−52	9	−36	−16
$\Delta_{\min}$	LDA[a]		−61	−22	−41
	LDA[b]			−45	−25
	LDA[c]				−30
	HF[a]	109	48	110	81
$\Delta_{\max}$	LDA[a]		61	24	35
	LDA[b]			64	43
	LDA[c]				20

Each datum in a row has been computed with reference to the set of vibrational frequencies (ω_v^{ref}) of the corresponding column. For example, the value −16 corresponds to $\Delta_{\min} = \min(\omega_v^{\mathrm{HF}} - \omega_v^{\mathrm{exp.}})$.
[a]Present work.
[b]Ref. 8.
[c]Ref. 7.
[d]Ref. 21.

Conclusions

The computational parameters on which the calculation of vibrational frequencies of a crystalline compound depend have been explored in the case of α-quartz. It has been possible to define a convenient set of parameters (including those controlling accuracy of the Coulomb and exchange series in HF, DFT grid, SCF convergence, accuracy of the geometry optimization, and in the numerical evaluation of the Hessian matrix) that provide numerically stable vibrational frequencies. When explored as a function of volume, these frequencies can be fitted to a low-order polynomial function, the fitting error being quite small. This will permit us to obtain an analytical representation of the vibrational contribution to thermodynamic functions and then minimize Gibbs free energy as a function of Volume (or pressure) and temperature.

HF and LDA hamiltonians have been compared with experiment. As expected, LDA performs slightly better than HF. When compared with previous calculations, our LDA results are on the whole closer to those obtained by Gonze et al.[7] However, the reason for the relative sparseness of LDA vibrational frequencies computed with different methods or by different authors is still not clear. The effect of basis set and the use of other Hamiltonians (in particular, B3-LYP, which has proved to perform very well in molecular calculations) need further investigation, also with reference to other systems.

On the basis of these satisfactory results it appears that frequency calculations for relatively large unit cell systems can be performed with high accuracy. This motivates us to complete the implementation of this set of features related to vibrational frequencies, namely the calculation of the non analytical part at Γ, the calculation of the infrared and RAMAN intensities, and the automatic generation of the dispersion spectrum both for comparison

with neutron scattering experiments and for the accurate evaluation of the thermodynamic functions.

References

1. Chalmers, J. M.; P. R. G., Eds. Handbook of Vibrational Spectroscopy; Wiley: Chichester, UK, 2001, vols. 4–5.
2. Frisch, M. J.; Trucks, G. W.; Schlegel, H. B.; Scuseria, G. E.; Robb, M. A.; Cheeseman, J. R.; Zakrzewski, V. G.; Montgomery, J. A., Jr.; Stratmann, R. E.; Burant, J. C.; Dapprich, S.; Millam, J. M.; Daniels, A. D.; Kudin, K. N.; Strain, M. C.; Farkas, O.; Tomasi, J.; Barone, V.; Cossi, M.; Cammi, R.; Mennucci, B.; Pomelli, C.; Adamo, C.; Clifford, S.; Ochterski, J.; Petersson, G. A.; Ayala, P. Y.; Cui, Q.; Morokuma, K.; Salvador, P.; Dannenberg, J. J.; Malick, D. K.; Rabuck, A. D.; Raghavachari, K.; Foresman, J. B.; Cioslowski, J.; Ortiz, J. V.; Baboul, A. G.; Stefanov, B. B.; Liu, G.; Liashenko, A.; Piskorz, P.; Komaromi, I.; Gomperts, R.; Martin, R. L.; Fox, D. J.; Keith, T.; Al-Laham, M. A.; Peng, C. Y.; Nanayakkara, A.; Challacombe, M.; Gill, P. M. W.; Johnson, B.; Chen, W.; Wong, M. W.; Andres, J. L.; Gonzalez, C.; Head–Gordon, M.; Replogle, E. S.; Pople, J. A. Gaussian 98, Revision A.11; Gaussian, Inc.: Pittsburgh, PA, 2001.
3. Schmidt, M. W.; Baldridge, K. K.; Boatz, J. A.; Elbert, S. T.; Gordon, M. S.; Jensen, J. J.; Koseki, S.; Matsunaga, N.; Nguyen, K. A.; Su, S.; Windus, T. L.; Dupuis, M.; Montgomery, J. A. J Comput Chem 1993, 14, 1347.
4. Stanton, J. F. Int J Quantum Chem 1991, 39, 19.
5. Deglmann, P.; Furche, F.; Ahlrichs, R. Chem Phys Lett 2002, 362, 511.
6. Baroni, S.; de Gironcoli, S.; Corso, A. D.; Giannozzi, P. Rev Mod Phys 2001, 73, 515.
7. Gonze, X.; Allan, D. C.; Teter, M. P. Phys Rev Lett 1992, 68, 3603.
8. Umari, P.; Pasquarello, A.; Corso, A. D. Phys Rev 2001, B 63, 094305.
9. Schütt, O.; Pavone, P.; Windl, W.; Karch, K.; Strauch, D. Phys Rev 1994, B 50, 3746.
10. Saunders, V. R.; Dovesi, R.; Roetti, C.; Orlando, R.; Zicovich–Wilson, C. M.; Harrison, N. M.; Doll, K.; Civalleri, B.; Bush, I. J.; D'Arco, P.; Llunell, M. CRYSTAL03 User's Manual; Università di Torino: Torino, 2003.
11. Doll, K.; Harrison, N. M.; Saunders, V. R. Int J Quantum Chem 2001, 82, 1.
12. Doll, K. Comp Phys Commun 2001, 137, 74.
13. Orlando, R.; Saunders, V. R.; Dovesi, R. unpublished.
14. Koch, W.; Holthausen, M. C. A Chemist's Guide to Density Functional Theory; Wiley-VCH Verlag GmbH: Weinheim, 2000.
15. Johnson, B. G.; Frisch, M. J. J Chem Phys 1994, 100, 7429.
16. Johnson, B. G.; Gill, P. M. W.; Pople, J. A. Chem Phys Lett 1994, 220, 377.
17. Martin, J. M. L.; Bauschlicher, C. W.; Ricca, A. Comp Phys Commun 2001, 133, 189.
18. Oganov, A. R.; Gillan, M. J.; Price, G. D. J Chem Phys 2003, 118, 10174.
19. Mehl, M. J.; Cohen, R. E.; Krakauer, H. J Geophys Res [Solid Earth] 1988, 93, 8009.
20. Gill, P. M. W.; Johnson, B. G.; Pople, J. A. Chem Phys Lett 1993, 209, 506.
21. Gervais, F.; Piriou, B. Phys Rev 1975, B 11, 3944.
22. Zakharova, E. K.; Zubov, V. G.; Osipova, L. P. Sov Phys Crystallogr 1975, 19, 489.
23. Monkhorst, H.; Pack, J. Phys Rev 1976, 13, 5188.
24. Saunders, V.; Freyria–Fava, C.; Dovesi, R.; Salasco, L.; Roetti, C. Mol Phys 1992, 77, 629.
25. Causà, M.; Dovesi, R.; Orlando, R.; Pisani, C.; Saunders, V. J Phys Chem 1988, 92, 909.
26. Pisani, C.; Dovesi, R.; Roetti, C. Lecture Notes in Chemistry; Springer Verlag: Heidelberg, 1988.
27. Becke, A. D. J Chem Phys 1988, 88, 2547.
28. Towler, M.; Zupan, A.; Causà, M. Comp Phys Commun 1996, 98, 181.
29. Saunders, V. R.; Orlando, R. unpublished.
30. Schlegel, H. B. J Comp Chem 1982, 3, 214.
31. Civalleri, B.; D'Arco, P.; Orlando, R.; Saunders, V. R.; Dovesi, R. Chem Phys Lett 2001, 348, 131.
32. Born, M.; Huang, K. Dynamical Theory of Crystal Lattices; Oxford Univ. Press: Oxford, 1954.
33. Catti, M. Lecture Notes in Chemistry; Springer Verlag: Berlin, 1996, p. 209.
34. Baranek, P.; Zicovich–Wilson, C.; Roetti, C.; Orlando, R.; Dovesi, R. Phys Rev 2001, B 64, 125102.
35. Noel, Y.; Zicovich–Wilson, C.; Civalleri, B.; D'Arco, P.; Dovesi, R. Phys Rev 2001, B 65, 014111.
36. Darrigan, C.; Rérat, M.; Mallia, G.; Dovesi, R. J Comp Chem 2003, 24, 1305.
37. Perdew, J. P.; Zunger, A. Phys Rev B 1981, 23, 5048.
38. Dirac, P. A. M. Proc Cambridge Phil Soc 1930, 26, 376.
39. Vosko, S.; Wilk, L.; Nusair, M. Can J Phys 1980, 58, 1200.